Materials and Design 160 (2018) 262–269

Contents lists available at ScienceDirect

Materials and Design

journal homepage: www.elsevier.com/locate/matdes

Environment-friendly and reusable ink for 3D printing of metallic structures

Chao Xu [a], Qinghua Wu [b], Gilles L'Espérance [c], Louis Laberge Lebel [a], Daniel Therriault [a,*]

[a] Department of Mechanical Engineering, Polytechnique Montreal, Montreal, QC H3T 1J4, Canada
[b] Department of Chemical Engineering, Polytechnique Montreal, Montreal, QC H3T 1J4, Canada
[c] Department of Metallurgy Engineering, Polytechnique Montreal, Montreal, QC H3T 1J4, Canada

HIGHLIGHTS

- An environment-friendly and reusable ink was developed for 3D printing of metallic structures.
- The metallic ink was printed at room temperature to build the 3D structure.
- The as-printed 3D structure was thermally treated to obtain a dense metallic structure.
- The fabricated structure after copper infiltration features a low filament porosity of 1.0%
- The copper infiltrated structures exhibit an electrical conductivity of 1.3×10^6 S/m and a Young's modulus of 160 GPa

GRAPHICAL ABSTRACT

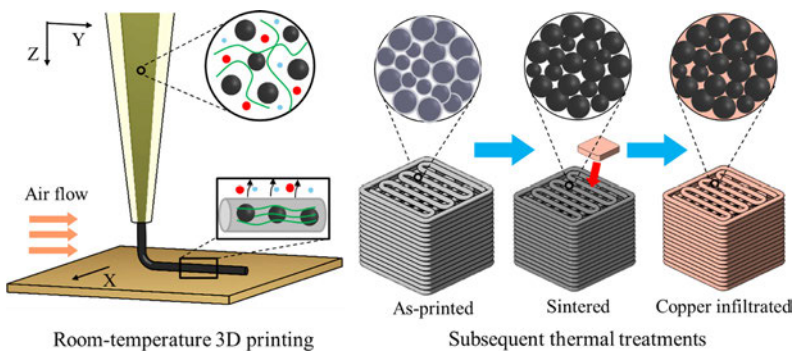

ARTICLE INFO

Article history:
Received 3 August 2018
Received in revised form 9 September 2018
Accepted 10 September 2018
Available online 13 September 2018

Keywords:
3D printing
Metallic ink
Environment-friendly
Metallic structures
Secondary metal infiltration

ABSTRACT

There is an increasing need for 3D printing of metallic structures in a green and cost-effective way. Here, an environment-friendly and reusable metallic ink was developed for an economical metal 3D printing method. The metallic ink is composed of steel micro powders, a biodegradable polymer: chitosan, acetic acid and deionized water. The metal 3D printing method consists of: (i) 3D printing of metallic structures using the metallic ink at room temperature, (ii) thermal treatments on the as-printed structures that decompose the polymer binder and sinter the steel powders, and (iii) an optional step: infiltrating melted copper into the sintered structures to achieve fully dense metal/metal hybrid structures. We demonstrate that any incorrectly built as-printed structures and scrap materials can be recycled and reused for 3D printing by dissolving them again in acetic acid. The fabricated structures after copper infiltration feature a low filament porosity of 1.0% which enables high properties such as an electrical conductivity of 1.3×10^6 S/m and a Young's modulus of 160 GPa. The metallic ink can be used for the 3D printing of high performance metallic structures while demonstrating a low environmental impact and a very effective utilization of metallic materials.

© 2018 Elsevier Ltd. This is an open access article under the CC BY-NC-ND license (http://creativecommons.org/licenses/by-nc-nd/4.0/).

1. Introduction

Additive manufacturing (AM) technologies, which build 3D structures layer-by-layer, provide a cost-effective alternative to create diverse metallic structures [1–3]. 3D printed metallic structures are used in a broad range of applications such as artificial bones as implants

* Corresponding author.
E-mail address: Daniel.therriault@polymtl.ca (D. Therriault).

https://doi.org/10.1016/j.matdes.2018.09.024
0264-1275/© 2018 Elsevier Ltd. This is an open access article under the CC BY-NC-ND license (http://creativecommons.org/licenses/by-nc-nd/4.0/).

[4–6], sensors [7,8], microelectronics [9,10], and batteries for energy storage [11,12]. The most commonly used commercial manufacturing technologies are powder-bed approaches such as selective laser sintering/melting (SLS/SLM) and electron beam melting (EBM) according to the fusion mechanism and energy source. In these technologies, fine micro scale metal powders are tightly compacted to form a powder bed. A high-intensity laser or electron beam selectively scans the powder particles to fuse them layer-by-layer [13]. Once completed, the fused part is removed from the powder bed and thoroughly cleaned by removing the loose or partially sintered powders. The advantages of SLS and SLM include high printing speed and high resolution. However, the nature of the powder bed methods prevents them from manufacturing various architectures such as enclosed and fine porous structures. The high power intensity laser system can be expensive and a safety hazard. Moreover, the repeated high-intensity scanning beam can cause the loss of alloying elements, a dramatic change in temperature (which can lead to metallurgy defects and residual stresses) and excessive oxidation [14–16].

Researchers attempted to address the shortcomings of the powder bed processes with direct energy deposition (DED), where a focused energy beam is utilized to fuse the metallic materials as they are being deposited. Skylar-Scott et al. sintered water-based silver inks using a focused laser as they were being extruded from the nozzle [17]. High resolution and freeform 3D metallic structures were manufactured using this technique. The electrical conductivity of the silver wires was 30% of that of bulk silver. However, this method was compatible with only a narrow range of low melting point metals such as silver. Although the mechanical properties were not reported in Ref. [17], given that water evaporation and the sintering of silver powders had to be accomplished within the limited time of laser scanning, the incomplete sintering might lead to poor mechanical properties of the final product. Furthermore, since this was a laser assisted process, it still suffered from the common laser induced limitations, like excessive oxidation and the loss of alloying elements.

Solvent-cast 3D printing (SC-3DP) consists of an ink paste containing metal powders, polymer and volatile solvent, in which no lasers or power beds are required [18]. The metallic ink is extruded through a micro nozzle under an applied pressure. The volatile solvent evaporates rapidly upon extrusion as a result of the pressure drop. The polymer solidifies and the rigidity of the extruded ink filament increases, which allows it to hold its shape and support the subsequent layers [18]. The result is a metal/polymer composite 3D structure. It is transformed into a metal structure through subsequent thermal treatments where the polymer is thermally decomposed and the metal powders are sintered. Xu et al. demonstrated the method using a metallic ink comprised of steel powders, polylactic acid (PLA) and dichloromethane (DCM), to create steel 3D structures [19]. Various structures were printed and they exhibited high mechanical and electrical performances, which were comparable with bulk materials. Jakus et al. reported the fabrication of metallic 3D structures employing metal oxides (i.e. Fe_2O_3, NiO and CuO) as the metal precursors [12]. The metal oxides were thermochemically reduced into sintered metal 3D structures in a reducing atmosphere of H_2. Although these processes are useful, like the majority of the SC-3DP approaches, the toxic and volatile DCM is used as the organic solvent. As a result, those processes have to be performed under a ventilation device because the toxic solvent can be harmful to the operator and the environment. Peng et al. introduced a water-based polymer solution to prepare metallic inks for SC-3DP, which is comprised of deionized water, polyvinyl alcohol (PVA) binder and polyethylene glycol (PEG) plasticiser [20]. Ferrite magnetic structures were fabricated by SC-3DP followed by a series of thermal treatments. However, the printed structures feature a low resolution of 0.6 mm with important shape deformation. As the volatility of the solvent and the pressure drop upon extrusion are the only triggers of solvent evaporation, the relatively long solidification time results in excessive sagging and deformation of the ink filament.

Driven by the aforesaid challenges, we developed an environment-friendly and reusable metallic ink compatible with the SC-3DP approach and subsequent thermal treatments (see Fig. 1). Highly alloyed steel (HAS) powders are uniformly mixed with a water-based polymer solution using a ball mill machine. The metallic paste, referred to the ink, is loaded into a syringe barrel and extruded through a tapered micro nozzle under a specific pressure at room temperature. A fan blows air over the extruded ink filament to accelerate solvent evaporation during the

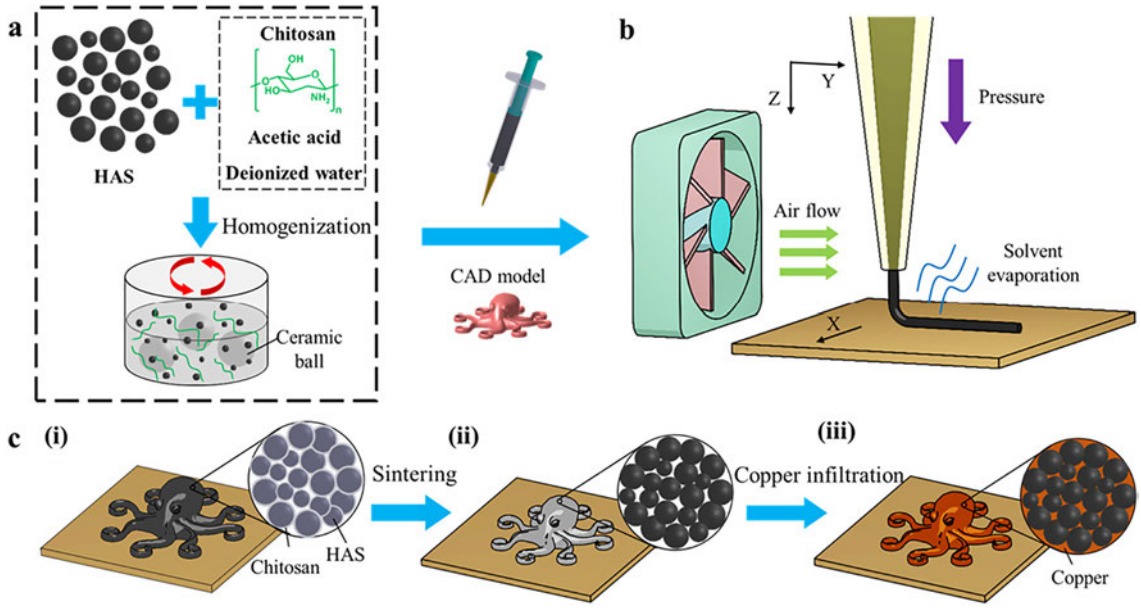

Fig. 1. Schematic of the fabrication process of a 3D metallic structure combining the following steps. (a) Metallic ink preparation: HAS powders are mixed with chitosan/acetic acid solution using a ball mill machine. (b) Solvent-cast 3D printing: the metallic ink is loaded in a syringe and extruded through a micro nozzle under a certain pressure at room temperature. The solvent content evaporates upon extrusion assisted by the flow of air. (c) Subsequent thermal treatments under Ar/H_2: (i) the dried as-printed sample is thermally treated in a furnace. (ii) The polymer is thermally decomposed and the HAS powders are sintered. (iii) After sintering, the sintered sample is infiltrated with melted copper, which fills the pores in the sintered filaments driven mainly by capillary forces.

extrusion. The ink filament is then deposited using a 3-axis robot at the specific coordinates according to the CAD model to create a 3D object. The as-printed sample is a hybrid metal/polymer 3D structure. After the part is dried in a vacuum oven at 50 °C for 2 h, it is thermally treated in an atmosphere containing Ar and H_2. The final product is a metal structure where the filament porosity can be tailored by the sintering duration [20]. A fully dense metallic structure is obtained by a copper infiltration process where the melted copper fills the pores inside the sintered filaments driven by capillary forces.

2. Experimental section

2.1. Ink preparation

The metallic material is a highly alloyed steel (HAS) micro powder with a spherical shape and a diameter less than 20 μm, which is the same powder as previously described in Ref. [19]. The chitosan is 90% deacetylated with an average molecular weight of 207 kDa, from Biolog in Germany. The acetic acid is purchased from Sigma-Aldrich and used as received. 0.8 g chitosan is dissolved in 10 mL 80 vol% acetic acid/deionized water. The chitosan solution is mixed using a ball mill mixer (8000M mixer/Mill, SPEX SamplePrep) for 10 min. After mixing, it is sealed and stored in a refrigerator. The metallic ink is prepared by mixing chitosan/acid solution with HAS powders at a weight ratio of 1:6.5 using the ball mill for 5 min. The detailed ink composition is summarized in Table 1.

2.2. 3D printing

3D printing is performed using a computer-controlled 3-axis positioning robot (I&J2200-4, I&J Fisnar) and a pressure dispensing system (HP-7X, EFD). The metallic ink is loaded into a syringe (3 mL, Nordson EFD) attached with a smooth-flow tapered nozzle (exit inner diameter = 250 μm). The structures are printed on a glass slide (PN 16004-422, VWR) with a thin layer of petroleum jelly (VSL-32600) as releasing agent. All the structures in this work are printed at a linear printing speed of 7 mm/s and under a pressure around 0.7 MPa, with an airflow system (a computer cooling fan, DC 12 V, 0.44A, flow rate = 800 L/min, 20 cm from the deposition nozzle). The layer height is 200 μm, 80% of the nozzle inner diameter. The layer thickness compensates for the filament reduction induced by solvent evaporation and guarantees secure, tight bonding between neighboring layers. The CAD models are either designed by a CAD software (CATIA) or downloaded from internet (thingiverse.com). They are sliced into several layers and interpreted into G-code by a slicing software (Simplify3D). Then the G-code is converted into a point-to-point program that can be read by the JR Points software to control the positioning robot.

2.3. Thermal treatments

The dried as-printed samples are thermally treated in a laboratory electric tubular furnace (59256-P-COM, Lindberg) on a ceramic substrate. The samples are prevented from oxidation by a circulated gas flow (97.5% Ar and 2.5% H_2, flow rate = 5 L/min) inside the quartz tube.

Table 1
Metallic ink composition for accurate printing.

Constituent	Density (g/ml)	Mass fraction (%)	Volume fraction (%)
Chitosan	1.4[a]	1.0	2.9
Acetic acid	1.05	10.0	40.8
Deionized water	1	2.4	10.2
HAS powders	8.05	86.7	46.1
Total	4.28	100.0	100.0

[a] The density of chitosan is the apparent density of chitosan in the as-printed sample.

2.4. Porosity analysis

The sintered and copper infiltrated scaffolds are sealed in a resin (EpoFix resin, Struers) block. The resin block is polished until the horizontal cross-section is visible. The cross-section is observed in an optical microscope (Zeiss Axioplan EL-Einsatz) and the amount of porosity is determined by an image analysis software (Clemex, ST-2000). The filament porosity is calculated as the ratio of void area inside the filament over the filament area. Ten cross-sections of each sample are analyzed.

2.5. Electrical conductivity measurement

The electrical conductivities of the sintered and copper infiltrated samples are measured using four-point probes method. The devices, circuit diagram and representative sample are shown in Fig. S4. A constant voltage of 0.1 V is provided by a power supply (Agilent, E3633A). The current and voltage are acquired by two multimeters (HP, 3457A). Five specimens of each sample type are tested.

2.6. Tensile test

The samples are sintered and copper infiltrated tensile bars, of which the cross-section of the neck is ≈3.6 × 1.6 mm. The filaments oriented +45°/−45° relative to the tensile direction, i.e. the filaments from odd number layers are +45° to the tensile direction, while the ones from even number layers are −45° to the tensile direction. The tensile tests are carried out on a MTS Insight machine with a 50 kN load cell (MTS 569332-01) at a crosshead speed of 1 mm/min and using an extensometer (gauge length = 8 mm, MTS 632.26, C-20). Five specimens for each sample type are tested.

3. Results and discussion

The spherical shape and the relatively small size of the HAS powders can enable low frictional forces between the micro powders and prevent the metallic ink from clogging the micro nozzle. Chitosan, a biocompatible polymer, can be dissolved in an acidic solution. Its solution was previously used to 3D print microstructures for guided cell growth [21]. Acetic acid is a volatile, organic, weak acid. Chitosan can be dissolved in an acetic acid water solution as a viscous hydrogel. Acetic acid is bio-compatible and evaporates rapidly in ambient conditions. Those features make chitosan/acetic acid a great candidate as a binder system for metal 3D printing.

Regarding the metallic ink formulation, the addition of excessive polymer binder results in incomplete dissolution. Part of the chitosan remains solid, which causes clogging of the micro nozzle. On the other hand, insufficient amount of polymer binder leads to brittle as-printed samples. The amount of deionized water is also an important parameter. Excessive water can increase the duration of solidification and result in sagging and shape deformation of the extruded ink filament mostly due to the slower evaporation rate of water compared to acetic acid. Nevertheless, insufficient water prevents the ionization of hydrogen ions from acetic acid, which can cause the incomplete dissolution of polymer.

The metallic ink is printed while a fan is blowing air on the ink filament upon extrusion. This enables faster solvent evaporation and thus, the solidification time of the extruded ink filament is shortened. The airflow setup, the influence of the airflow on the solvent evaporation speed and the printing quality are shown in Fig. S1 and Video S1. The solvent evaporation speed is investigated by weighing the extruded ink filaments printed with and without the airflow. Half of the solvent content (acetic acid and deionized water) evaporates within 168 s after extrusion without airflow. On the other hand, it only takes 66 s assisted by the airflow, which improves the solvent evaporation speed by 2.5 times. Due to the short solidification time, the ink filament does not sag, flow or merge with neighboring filaments. By comparing the printing process and the as-printed scaffolds, it is clearly observed that

the one printed with airflow assistance proves to be more reliable. The one printed without airflow, however, has merged filaments and loses its shape. To ensure the printing quality, all the structures in this work are printed with a tapered nozzle (tip inner diameter: 250 μm) at a linear printing speed of 7 mm/s with the airflow assisted.

During printing the samples, it was difficult to release the sample from the substrate. For the releasing purpose, a thin layer of Petroleum jelly is applied on the substrate prior to printing. Once the printing is completed, the sample along with the substrate is placed in a vacuum oven at 50 °C for 2 h. The petroleum jelly melts and acts as a lubrication between the bottom of the sample and the substrate. The sample can be easily released from the substrate. After drying in the vacuum oven, the diameter of the filament is around 220 μm, which is 88% of the nozzle inner diameter. Fig. 2a–e shows scanning electron microscope (SEM) images of a dried as-printed scaffold, including the structure, the filament and the HAS micro particles. The images of the as-printed samples demonstrate the versatility of our 3D printing method to fabricate well-organized structures from the metallic ink. The structure is qualitatively ordered (Fig. 2a). The filaments from neighboring layers are perpendicularly stacked without shape deformation (Fig. 2b). As the metal content is up to 94.1 vol% in the dried as-printed sample, the filament is comprised of mainly HAS powders covered and bound by a thin layer of chitosan (Fig. 2c–d). There are small fragments (≈0.5 μm) randomly distributed on the surface of the HAS particle (Fig. 2e). The HAS particle retains its spherical shape without visible chemical corrosion induced pits on the surface. To investigate the composition of the small fragments, an energy dispersive X-ray spectroscopy (EDS) analysis is carried out on the HAS particle (Fig. 2f). The small fragments on the HAS particle surface contain more carbon and oxygen compared to the rest of the area on the HAS particle surface. It suggests that they should be the aggregates of the precipitated chitosan after the solvent evaporates. As a result, although the metallic ink contains metal powders and weak acid, it is chemically stable at room conditions.

The 3D structures printed from the metallic ink are reusable (Fig. S2). Any incorrectly printed structures and scrap materials can be dissolved in the acid solvent in a proportion according to the ink recipe (Table 1) and then mixed using the ball mill. After homogenization, the recycled metallic ink can be reused for 3D printing. In addition, the manufacturing efficiency can be improved by using multiple printheads (including a pressure dispensing system, syringe holder, syringe and micro nozzle) (Video S2). By adjusting the nozzle tips to the same height, multiple copies of the structures can be printed at the same time. If different inks are loaded in different syringe, multiple copies of the structures made in different materials can be printed at one time.

To determine the temperature profile of the thermal treatments, the decomposition temperatures of the polymer binders are investigated by conducting thermal gravity analysis (TGA) in a nitrogen atmosphere (Fig. 3a). The commonly used polymer binder, PLA, degrades below 400 °C. Chitosan loses 10% of its weight under 100 °C due to loss of moisture. It partially decomposes at around 300 °C where the weight drops by another 40%. Then the decomposition speed slows down and around 30% of the weight is left until 800 °C. It coincides with the results reported by the previous researcher [22]. The residues (Fig. 3b) contains mainly carbon according to the elemental test result. The carbon can diffuse into the HAS powders during the thermal treatments, hardening the sintered steel [23]. The petroleum jelly, which acts as the releasing agent, completely decomposes at around 400 °C. Fig. 3c shows the sintering temperature profile which consists of a polymer debinding plateau at 400 °C for 1 h and a metal sintering plateau at 1165 °C for 3 h. If the samples are prepared for copper infiltration, the sintering plateau at 1165 °C only lasts for 1 h. The shorter sintering duration leaves more pores within the filaments for the melted copper infiltration. The copper infiltration is conducted on the sintered structures at 1120 °C for 1 h by placing a piece of infiltrating copper on the top of the sintered sample (Fig. 3c). The amount of the copper is calculated according to the filament porosity and filament volume. Fig. 3d shows the as-printed, sintered and copper infiltrated scaffolds thermally treated following this temperature profile.

To determine the performance of chitosan/acetic acid as a polymer binder solution, the properties of sintered and copper infiltrated samples (printed from chitosan/acetic acid based metallic ink, hereafter referred to CHI) and samples (printed from PLA/DCM based metallic ink, hereafter referred to PLA) are compared. The comparison is based on the optimized ink recipes (CHI and PLA) for best printing quality. The results of ink filament morphology, filament porosity, size reduction and electrical properties are shown in Fig. 4. The SEM images of sintered

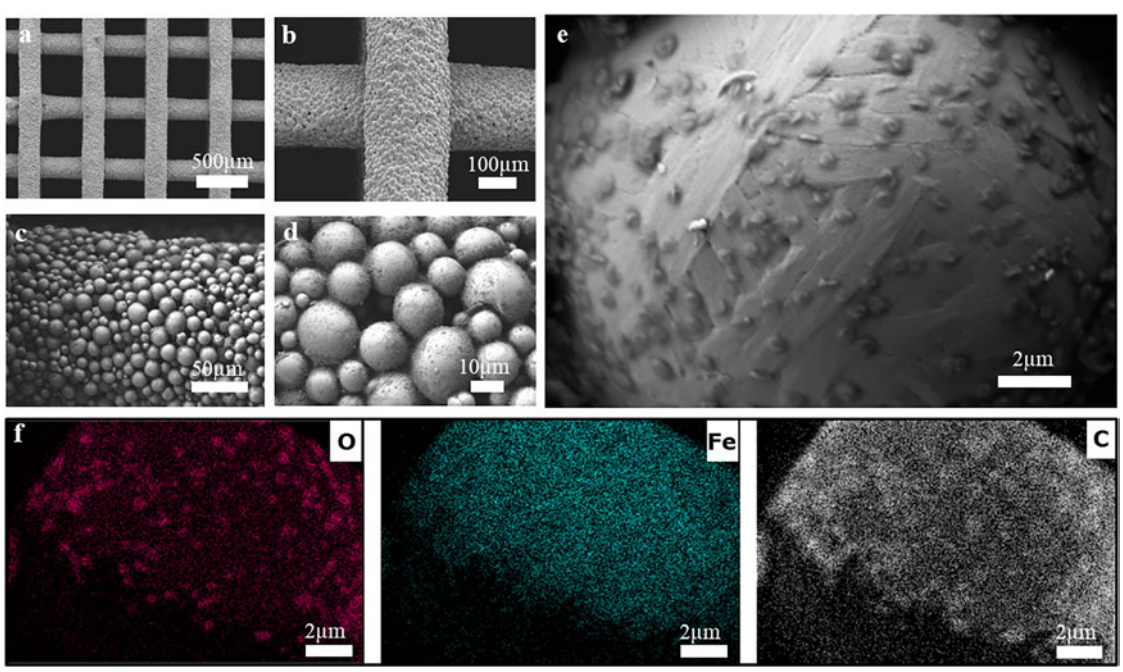

Fig. 2. Scanning Electron Microscope (SEM) images of as-printed scaffolds (tapered nozzle: 250 μm in diameter) at different magnifications: (a), (b), (c), (d), of a single HAS particle of the dried as-printed scaffold (e), and (f) energy dispersive X-ray spectroscopy (EDS) results of oxygen, iron and carbon on the single HAS particle.

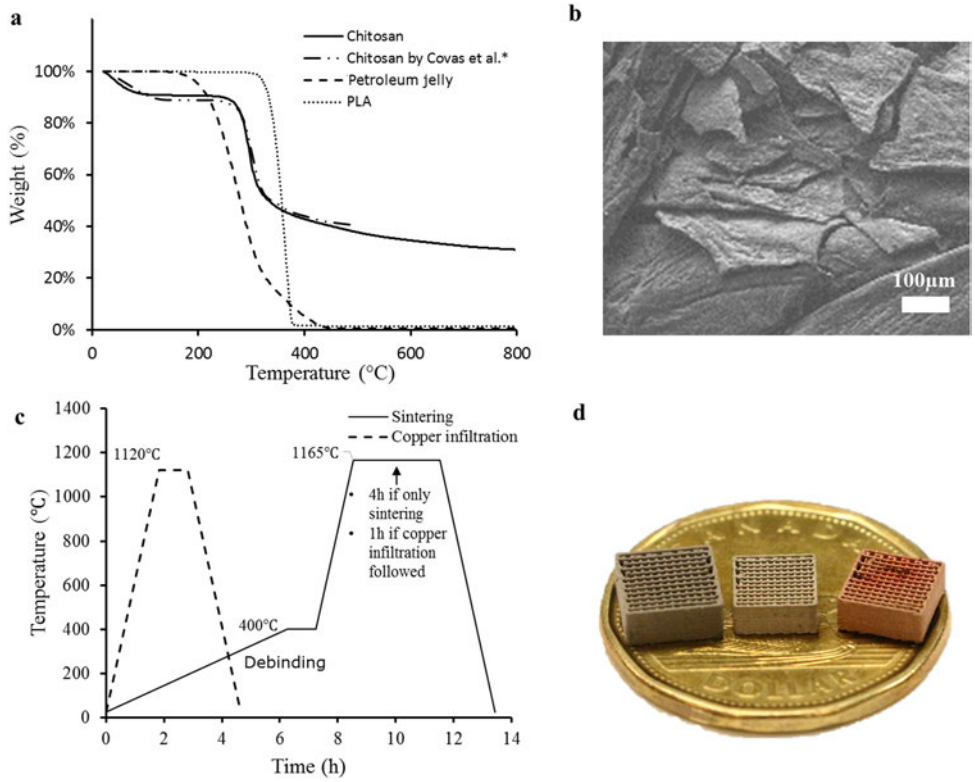

Fig. 3. (a) TGA results of chitosan [22], PLA and petroleum jelly in nitrogen up to 800 °C, (b) the SEM image of the chitosan thermal decomposition residues, (c) temperature profiles of the thermal treatment processes, and (d) the optical image of the as-printed, sintered and copper infiltrated scaffolds.

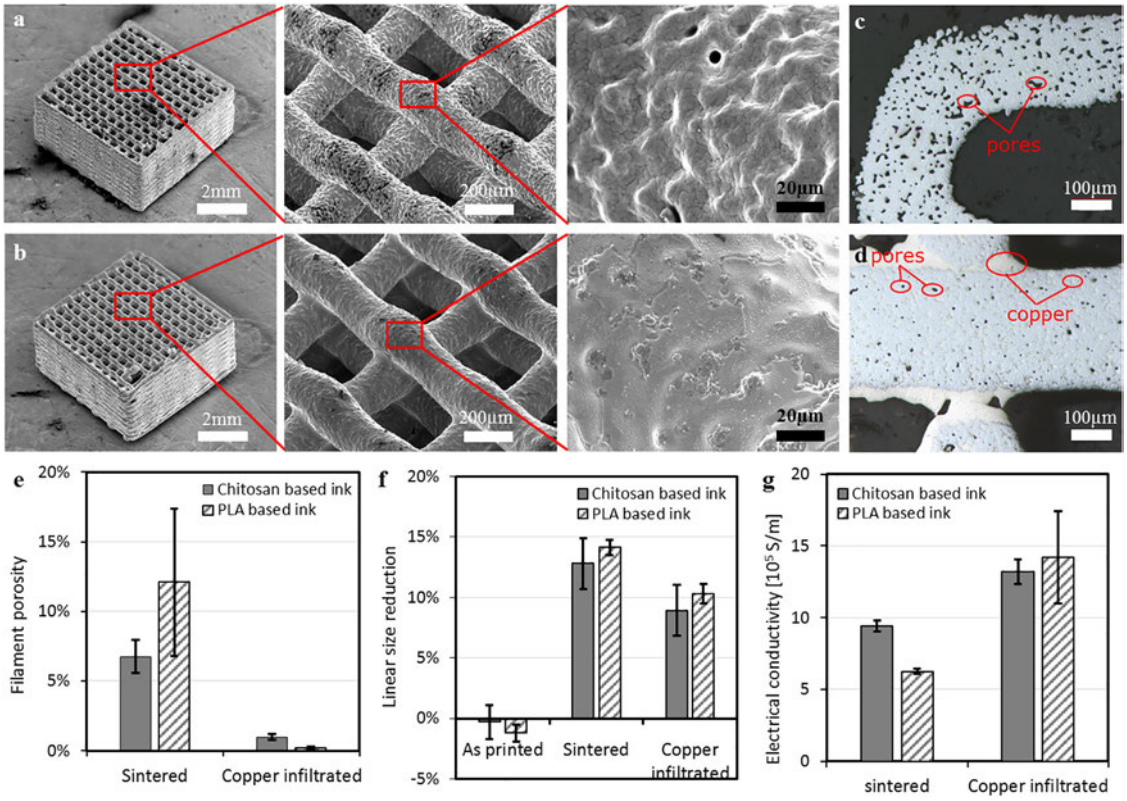

Fig. 4. SEM images of (a) sintered and (b) copper infiltrated CHI scaffolds at different magnifications and optical image of polished filament cross-section of (c) sintered and (d) copper infiltrated samples. (e) The filament porosity, (f) linear size reduction and (g) electrical conductivity of sintered and copper infiltrated scaffolds printed from chitosan based metallic ink and PLA based metallic ink [19].

and copper infiltrated scaffolds (CHI) reveal the finer details of the structure, filaments and fused metal powders (Fig. 4a–b). Both scaffolds keep the shape from the as-printed scaffold (Fig. 2a) without distortion and the filaments are aligned uniformly and well organized. The individual filament has cylindrical shape. No obvious deformation is observed even for spanning structure. The filament porosity is studied by analyzing the optical microscope images of the cross-section of the sintered and copper infiltrated scaffolds (Fig. 4c–d). The filaments of the copper infiltrated scaffold show better bonding between neighboring layers than those from sintered ones. It is observed that the melted copper only fills the pores inside the filament, not the space between deposited filaments. By properly tailoring the amount of copper, the copper infiltration can be applied to enhance the fine porous structure [19].

The metal powders fuse together through the sintering, but there are some pores left in the sintered filaments due to the removal of the polymer binder and sintering itself. The pores can be filled by melted copper and the filament surface becomes smoother. Pores of similar sizes are uniformly scattered inside the sintered filament. In the copper infiltrated scaffold, melted copper fills most of the pores in the filaments and the gap between contacting filaments. The porosity significantly decreases after copper infiltration. The filament porosities of sintered and copper infiltrated samples are 6.8% ± 1.2% and 1.0% ± 0.2% respectively (Fig. 4e and Table S1). Compared to the structures (PLA) in our previous work [19], the sintered scaffold (CHI) has less porosity, while the copper infiltrated one exhibits slightly higher porosity. The reason is that the polymer content of the as-printed samples (CHI) (6 vol%) is much lower than that of the as-printed samples (PLA) (25 vol% [19]). After polymer decomposition, there are less pores resulting from removing the polymer. The sintered filament (CHI) achieves less porosity after sintering at the same conditions and duration. Less porosity hinders the melted copper from infiltrating into the sintered filaments in the subsequent copper infiltration. It results in higher porosity than the one printed from PLA based ink, but it is still around 1% porosity.

Fig. 4f shows the linear size reduction of the as-printed, sintered and copper infiltrated samples (CHI and PLA) compared to the designed size. The size changes are caused by the expansion upon extrusion, solvent evaporation, polymer decomposition, sintering and copper infiltration. Table S2 summarizes the linear size reduction values. The extruded ink filament expands because of the pressure drop and then shrinks due to the solvent evaporation. The dried as-printed CHI sample has similar size as designed (0.3% ± 1.4% linear expansion). After polymer decomposition and metal sintering, the sintered structure exhibits a linear reduction of 12.8% ± 2.1% compared to the designed size. The copper infiltrated sample has a sintering duration for 1 h instead of 3–6 h for the sintered samples. More pores are left to allow the melted copper to infiltrate into the sintered filament easily. As a result, the copper infiltrated sample exhibits less size reduction (8.9% ± 2.1% linear reduction) than the sintered one. The samples (CHI) have less size change compared to the samples (PLA) in every stage, as they contain less polymer contents. The size reduction in three dimensions is also studied. The results (Fig. S3) indicate that the size reduction does not show significant differences along the directions.

The sintered and copper infiltrated samples (CHI) have the electrical conductivity of $(9.4 \pm 0.4) \times 10^5$ S/m and $(1.3 \pm 0.9) \times 10^6$ S/m, respectively (Fig. 4g and Table S3). Compared to the samples (PLA), the sintered samples (CHI) are 51% more conductive. In CHI ink, the polymer volume fraction is lower. As a result, the sintered sample (CHI) has denser structure resulting in a higher electrical conductivity. The copper infiltrated samples (CHI) have the same conductivity within error as the PLA samples, but with a smaller error bar. The sintered samples (CHI) has a narrower range in filament porosity and therefore the electrical conductivity as compared to the PLA samples.

Tensile tests are conducted on the sintered and copper infiltrated tensile bars to investigate their mechanical properties. Fig. 5 shows the representative tensile stress-strain curves, optical images of representative tensile bars and SEM images of the tensile fracture surfaces. The observed Young's modulus *E*, ultimate tensile strength (UTS) and elongation at breakage (%) are summarized in Table S4. The previous tensile test results of the samples printed from PLA base ink are also listed for comparison [19]. The *E* modulus of the sintered samples (CHI) is ~205 GPa, which is improved by 5% when compared with the samples printed from PLA based ink. The UTS and elongation at break, however, are decreased by 32% and 60% respectively. The stiffness (*E*) is increased, while the ductility (UTS and elongation at break) is sacrificed. Compared to the sintered samples, the copper infiltrated samples (CHI) exhibit better UTS (522 MPa) and elongation at break (0.69%). The infiltrated copper improves the ductility of the sintered samples. As the copper infiltrated samples go through a shorter sintering duration (1 h), the *E* modulus (160 GPa) is lower than the sintered ones. As the chitosan binder can introduce extra carbon to the sintered metal structure, it hardens the structure, but reduces the ductility during sintering. The binder might be more suitable for low carbon content metal alloys, where it could improve the stiffness without sacrificing the ductility.

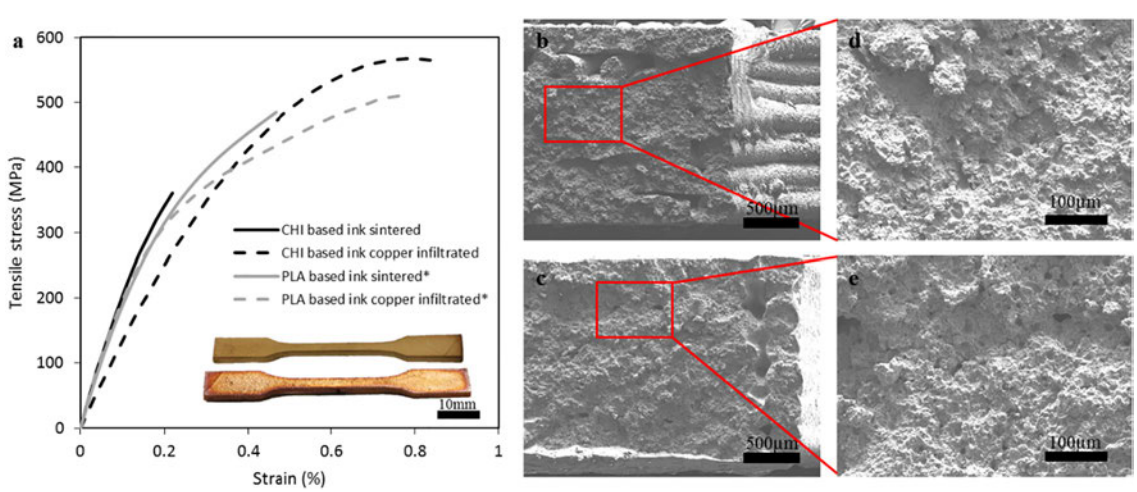

Fig. 5. (a) Tensile stress versus strain curves for sintered and copper infiltrated tensile samples printed using chitosan based ink and PLA based ink [19] and optical image of sintered and copper infiltrated tensile samples (inset). SEM images of tensile fracture surfaces of CHI sintered and copper infiltrated tensile bars at (b, c) low and (d, e) higher magnification, respectively.

The tensile fracture surfaces of the sintered and copper infiltrated samples are studied for better understanding the mechanism (Fig. 5b–e). In the sintered sample (Fig. 5b), most of the filaments from the same and different layers merge together, although some tiny pores are left in the structure. The copper infiltrated sample (Fig. 5c) has a denser structure. The high magnification SEM images (Fig. 5d–e) show the details of the tensile fracture surface. All the metal powders fuse and merge together. No individual metal particle is visible under SEM. The structure is a single entity with few tiny pores. The tensile fracture surface images show that the sintered and copper infiltrated samples (CHI) are much denser than those of PLA samples because the CHI metallic ink has a much higher volume fraction of metal than the PLA ink.

Fig. 6 presents various 3D metallic structures fabricated using our green ink and Video S3 shows the printing process in motion. As-printed and sintered 3D structures are shown in Fig. 6a. Relatively complex structures, such as the octopus and skull, can be easily printed and maintain their fine features after sintering in spite of a size reduction. The size reduction appears to be reproducible for a specific temperature profile and could be compensated by introducing an offset in the design stage. Fig. 6b shows fully dense sintered structures including a replica of Mayan pyramid and a pair of elliptical gears. The steps along the side of the pyramid are clear and the corners are relatively sharp. The elliptical gears mesh well with each other without any post sintering surface treatments. Our extrusion-based approach is also compatible with the fabrication of porous metallic structures, not always possible with power-bed methods. A fine porous femur bone with a designed porosity of 50% is fabricated (see Fig. 6c). The pores and tunnels in the structure are designed in the CAD model. The filling density can be tailored from 20% to 100% using the slicing software, achieving a porous structure with desired effective stiffness and weight. The porous structures are printed at room-temperature and can withstand subsequent sintering. 3D twisted vases with a porous infill and a solid surface layer are shown in Fig. 6d. Their surface is smoother than porous structures and they weigh less than fully dense structures. However, the structures without a flat bottom surface have to be printed with the assistance of supporting structures (e.g. the femur bone in Fig. 6c).

4. Conclusion

We have developed an environment-friendly and reusable metallic ink for 3D printing of highly dense metallic structures. The metallic ink contains steel micro powders, a biodegradable polymer: chitosan, acetic acid and deionized water. It can be applied in a low-cost SC-3DP method to fabricate metallic structures and overcome the use of toxic solvent. The ink is reusable which improves the metallic materials utilization. An airflow system is used to counterbalance the shortcomings of SC-3DP methods by accelerating solvent evaporation and shortening the solidification duration of the extruded ink filament, reducing the sagging and the shape deformation. The morphology, size reduction, filament porosity, electrical conductivity and mechanical properties of the fabricated structures are characterized. Comparing with commonly used more toxic PLA/DCM based metallic ink, our ink produces 3D metal structures with less size reduction, lower filament porosity while demonstrating comparable electrical and mechanical performances. We envision that the chitosan polymer solution system could apply to diverse metallic materials, metal oxides and ceramics to obtain green and reusable 3D-printable inks. The structures built using this approach can be potentially used in biomedical and aerospace fields since geometrically complex shapes are porous configurations are often preferred. We foresee that artificial bone implants with fine and uniform pores, as well as complex 3D porous aerospace structures featuring light weight and high mechanical performance can be fabricated using this ink in a very economical fashion.

Supplementary data to this article can be found online at https://doi.org/10.1016/j.matdes.2018.09.024.

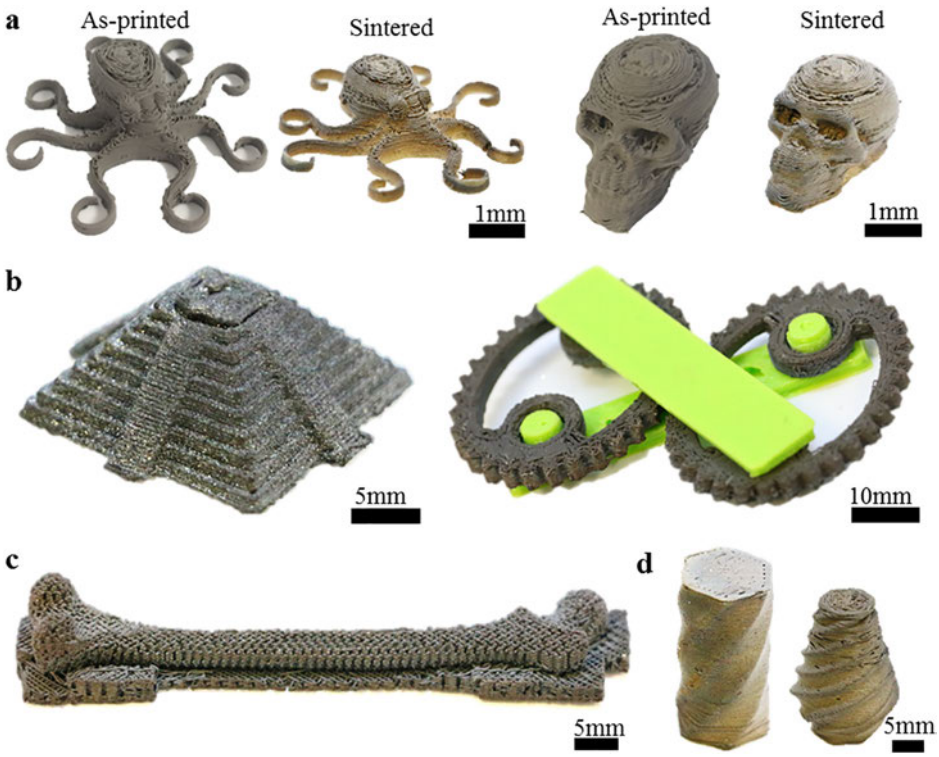

Fig. 6. Various 3D printed structures, including (a) as-printed and sintered octopus and skull, (b) fully dense sintered structures: a replica of Mayan pyramid and a pair of elliptical gears, (c) a porous femur bone with a designed porosity of 50%, and (d) twisted vases with a porous infill and a solid surface layer.

Data availability

The raw/processed data required to reproduce these findings can't be shared at this time as the data also forms part of an ongoing study.

Authors' contributions

1. Chao Xu, Daniel Therriault and Louis Laberge Lebel proposed the idea of environment-friendly metallic ink for 3D printing.
2. Chao Xu conducted the experiments, analyzed the data and wrote this manuscript,
3. Qinghua Wu provided advice on the polymer binder solution,
4. All the authors gave a lot of constructive discussions and reviewed the manuscript.

Acknowledgements

The authors acknowledge the financial support from NSERC (Natural Sciences and Engineering Research Council of Canada, grant number: RGPIN 312568-2013) and Auto 21 of the Networks of Centres of Excellence of Canada (NCE) program. A scholarship for Mr. Xu was also provided by the China scholarship Council (CSC) and the Fonds de recherche du Quebec - Nature et technologies (FRQNT).

References

[1] J.H. Martin, B.D. Yahata, J.M. Hundley, J.A. Mayer, T.A. Schaedler, T.M. Pollock, 3D printing of high-strength aluminium alloys, Nature 549 (2017) 365–369.
[2] J.R. Greer, J. Park, Additive manufacturing of nano-and microarchitected materials, Nano Lett. (4) (2018) 2187–2188.
[3] T. DebRoy, H.L. Wei, J.S. Zuback, T. Mukherjee, J.W. Elmer, J.O. Milewski, A.M. Beese, A. Wilson-Heid, A. De, W. Zhang, Additive manufacturing of metallic components–process, structure and properties, Prog. Mater. Sci. 92 (2018) 112–224.
[4] S. Bose, D. Ke, H. Sahasrabudhe, A. Bandyopadhyay, Additive manufacturing of biomaterials, Prog. Mater. Sci. 93 (2018) 45–111.
[5] X. Wang, S. Xu, S. Zhou, W. Xu, M. Leary, P. Choong, M. Qian, M. Brandt, Y.M. Xie, Topological design and additive manufacturing of porous metals for bone scaffolds and orthopaedic implants: a review, Biomaterials 83 (2016) 127–141.
[6] A. Basalah, Y. Shanjani, S. Esmaeili, E. Toyserkani, Characterizations of additive manufactured porous titanium implants, J. Biomed. Mater. Res. Part B 100 (2012) 1970–1979.
[7] R. Bernasconi, F. Cuneo, E. Carrara, G. Chatzipirpiridis, M. Hoop, X. Chen, B.J. Nelson, S. Pané, C. Credi, M. Levi, L. Magagnin, Hard-magnetic cell microscaffolds from electroless coated 3D printed architectures, Mater. Horiz. 5 (2018) 699–707.
[8] Y.S. Rim, S.H. Bae, H. Chen, N.D. Marco, Y. Yang, Recent progress in materials and devices toward printable and flexible sensors, Adv. Mater. 28 (2016) 4415–4440.
[9] A. Vyatskikh, S. Delalande, A. Kudo, X. Zhang, C.M. Portela, J.R. Greer, Additive manufacturing of 3D nano-architected metals, Nat. Commun. 9 (2018) 593.
[10] D.W. McOwen, S. Xu, Y. Gong, Y. Wen, G.L. Godbey, J.E. Gritton, T.R. Hamann, J. Dai, G.T. Hitz, L. Hu, Eric.D. Wachsman, 3D-printing electrolytes for solid-state batteries, Adv. Mater. (2018), 1707132.
[11] B.M. Sánchez, Y. Gogotsi, Synthesis of two-dimensional materials for capacitive energy storage, Adv. Mater. 28 (2016) 6104–6135.
[12] A.E. Jakus, S.L. Taylor, N.R. Geisendorfer, D.C. Dunand, R.N. Shah, Metallic architectures from 3D-printed powder-based liquid inks, Adv. Funct. Mater. 25 (2015) 6985–6995.
[13] R.D. Farahani, M. Dubé, D. Therriault, Three-dimensional printing of multifunctional nanocomposites: manufacturing techniques and applications, Adv. Mater. 28 (2016) 5794–5821.
[14] H. Gong, K. Rafi, H. Gu, G.D.J. Ram, T. Starr, B. Stucker, Influence of defects on mechanical properties of Ti–6Al–4V components produced by selective laser melting and electron beam melting, Mater. Des. 86 (2015) 545–554.
[15] E.O. Olakanmi, R.F. Cochrane, K.W. Dalgarno, A review on selective laser sintering/melting (SLS/SLM) of aluminium alloy powders: processing, microstructure, and properties, Prog. Mater. Sci. 74 (2015) 401–477.
[16] R. Chou, J. Milligan, M. Paliwal, M. Brochu, Additive manufacturing of Al-12Si alloy via pulsed selective laser melting, JOM 67 (2015) 590–596.
[17] M.A. Skylar-Scott, S. Gunasekaran, J.A. Lewis, Laser-assisted direct ink writing of planar and 3D metal architectures, Proc. Natl. Acad. Sci. 113 (2016) 6137–6142.
[18] A.B. Yeop, D. Shoji, C.J. Hansen, E. Hong, D.C. Dunand, J.A. Lewis, Printed origami structures, Adv. Mater. 22 (2010) 2251–2254.
[19] C. Xu, A. Bouchemit, G. L'Espérance, L.L. Lebel, D. Therriault, Solvent-cast based metal 3D printing and secondary metallic infiltration, J. Mater. Chem. C 5 (2017) 10448–10455.
[20] E. Peng, X. Wei, T.S. Herng, U. Garbe, D. Yu, J. Ding, Ferrite-based soft and hard magnetic structures by extrusion free-forming, RSC Adv. 7 (2017) 27128–27138.
[21] Q. Wu, M. Maire, S. Lerouge, D. Therriault, M.C. Heuzey, 3D printing of microstructured and stretchable chitosan hydrogel for guided cell growth, Adv. Biosyst. 1 (2017), 1700058.
[22] C. Peniche-Covas, W. Argüelles-Monal, J.S. Román, A kinetic study of the thermal degradation of chitosan and a mercaptan derivative of chitosan, Polym. Degrad. Stab. 39 (1993) 21–28.
[23] E.P. DeGarmo, J.T. Black, R.A. Kohser, B.E. Klamecki, Materials and Process in Manufacturing, Prentice Hall, 1997.